A Multi-modal Sensor Array for Safe
Human-Robot Interaction and Mapping

Colette Abah[1], Andrew L. Orekhov[1], Garrison L.H. Johnston[1], Peng Yin[2], Howie Choset[2], Nabil Simaan[1†]

Abstract— In the future, human-robot interaction will include collaboration in close-quarters where the environment geometry is partially unknown. As a means for enabling such interaction, this paper presents a multi-modal sensor array capable of contact detection and localization, force sensing, proximity sensing, and mapping. The sensor array integrates Hall effect and time-of-flight (ToF) sensors in an I^2C communication network. The design, fabrication, and characterization of the sensor array for a future *in-situ* collaborative continuum robot are presented. Possible perception benefits of the sensor array are demonstrated for accidental contact detection, mapping of the environment, selection of admissible zones for bracing, and constrained motion control of the end effector while maintaining a bracing constraint with an admissible rolling motion.

Index Terms— Robot perception, Collaborative robots, Continuum robots, Bracing, Mapping.

I. INTRODUCTION

Industrial workers often perform tasks in close quarters. For example, manufacturing/service tasks within airplanes, power plants, and ships involve operating in confined spaces that may require many customization steps, including fitting of hydraulic/fuel pipes, running new cables, welding of gussets, and deployment of thermal insulation/sealants.

These examples take place in constrained quarters that require workers to operate in unnatural postures, causing them fatigue and injury. OSHA, citing Bureau of Labor Statistics [1], estimates that over 600,000 work-related musculoskeletal disorders account for 34% of lost workdays. The physical risk factors contributing to work related musculoskeletal disorders (WMD) are well documented, including holding un-ergonomic positions, exerting sustained forces, motion repetition, tool vibration, and managing heavy tools, especially when such factors are combined [1]. These factors are exacerbated when workers operate in confined spaces.

Robots capable of supporting loads and performing repetitive tasks are envisioned as a means for reducing the risk of WMDs. In contrast to manufacturing tasks in open structured environments where robots have been used autonomously

or more recently in cooperation (close proximity) with workers [2–4], cooperative manufacturing in confined spaces demands new cooperation modes with levels of dexterity, sensing, and safety that exceed the capabilities of existing robotic systems. While a telemanipulation interface could enable the user to control the robot from outside the confined space (*ex-situ* collaboration), this control strategy may not be acceptable in some scenarios where human sensory presence is key to quality control and successful completion of complex service tasks. Additionally, most applications that would require robot assistance within a confined space involve operation within semi-structured environments where the basic geometry is known based on the nominal manufacturing plan, but the actual environment differs from this *a priori* plan due to manual customizations (e.g. passing new wire harnesses, pipes and air conditioning ducts). Therefore, there is a need for *in-situ collaborative robots* (ISCRs) that are safe enough to operate within a confined space while allowing the co-located worker to retain their sensory presence and to use intuitive control, e.g. through an admittance (cooperative) control of the robot.

ISCRs must be able to reach deep within confined spaces while maintaining end effector payload capabilities and precision. One means for achieving this functional requirement is through the use of snake-like structures (also known as continuum robots [5]), augmented with the ability to brace against the environment. Such designs have the advantage of requiring less powerful motors, which may contribute to increasing user safety and reducing bulk. In addition, these robots must be able to detect objects in their environments (humans and other objects) to enforce safety rules, as well as select admissible regions for bracing. Furthermore, the robots must allow safe interaction along their entire length and offer both active and passive safety features in case of accidental collision.

While this paper focuses entirely on the sensor design and preliminary evaluation, our envisioned concept for one of the key building block of ISCRs is a continuum robot equipped with an array of sensors, as illustrated in Fig. 1. Continuum robots offer passive safety due to their inherent compliance. To make such robots even safer around humans and to endow them with situational awareness, we propose the use of multi-modal sensing disk units (SDUs) capable of proximity sensing, mapping of the environment, contact detection and localization, and force sensing.

There have been prior works on force sensing and contact detection in the context of continuum robots. Most research efforts have focused on calculating the wrench of the end

effector of continuum robots by measuring the load at the actuation lines [6], measuring the deflection from equilibrium position [7–9], or using helical FBG sensors [10]. Kinematic-based contact detection along the body of a multi-backbone continuum robot has also been investigated in [11]. The sensor design in this paper provides force, contact, and proximity information along the body of a continuum robot without relying on kinematics-based detection or deflection modeling. This additional sensory input can improve environment interaction performance [12] and potentially provide a means for calibrating the continuum robot's shape by registering the robot to the environment.

There is an extensive literature on robotic skins. Sources [13] and [14] provide a more complete picture of these works. Several relevant works on multi-modal robotic skins [15–19] have integrated various combinations of proximity sensing, contact detection, and normal force sensing to equip robots with tactile sensing capabilities. Our design builds on these prior works; in addition to proximity and force sensing capabilities, we propose to augment continuum robots with whole-body mapping and force localization capabilities. To the best of our knowledge, this multi-modal sensory disk is novel, and its planned combination within the context of intelligent continuum robots for manufacturing and safe human-robot interactions in confined spaces has not been presented or evaluated.

The rest of this paper is structured as follows; first we present the details of the design and fabrication of the sensing disk unit. Next, we present the results of a preliminary characterization of the sensing disk unit. Finally, we demonstrate the use of the sensor disk mounted on an industrial robot for mapping of an environment, selection of an admissible bracing region, and safe bracing.
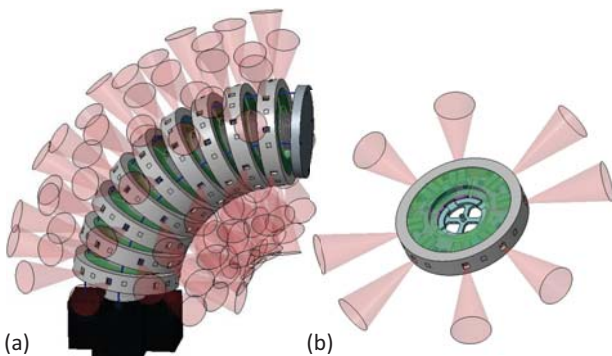

Fig. 1: (a) Continuum segment augmented with proximity sensing, mapping, force sensing, and localized contact detection capabilities. (b) Multi-modal sensing disk unit (SDU).

II. SENSOR ARRAY DESIGN

The mechanical architecture of continuum robots is such that spacer disks are used as passive elements on which a central backbone is mounted, and through which secondary backbones slide to achieve controlled bending in different directions (e.g. [20], [21]). In this work, we propose to

augment continuum robots with situational awareness by substituting passive spacer disks with multi-modal sensing disks units (SDUs), as shown in Fig. 1. These SDUs will enable the continuum robot to sense proximity, map its environment, detect and localize contact, and sense force.

Figure 2 shows the design and a prototype of the SDU. Each SDU includes eight time-of-flight sensors and eight Hall effect sensors assembled onto two half rings, two custom printed circuit boards (PCBs) for signal multiplexing and communication, and a protective silicone sleeve that houses the magnets for Hall effect sensing. The sensors are distributed in a circular pattern that leaves room for the passing of secondary backbones (of a continuum robot).

For proximity sensing and mapping, we use an array of VL6180X time-of-flight (ToF) sensors from ST Microelectronics. This sensor computes the absolute distance of the nearest object by measuring the time the light takes to travel to the object and back to the sensor. The specified range for the VLX180 is 0 to 100 mm, which is useful for detecting objects in close proximity to the continuum robot. The detection cones of these proximity sensors along the body of the continuum robot are illustrated in Fig. 1. In the future, SDUs will include long-range sensors (e.g. VL53L0X) along with the current short-range sensors in an alternating pattern that enables dual-range proximity sensing and mapping of the environment in confined spaces.
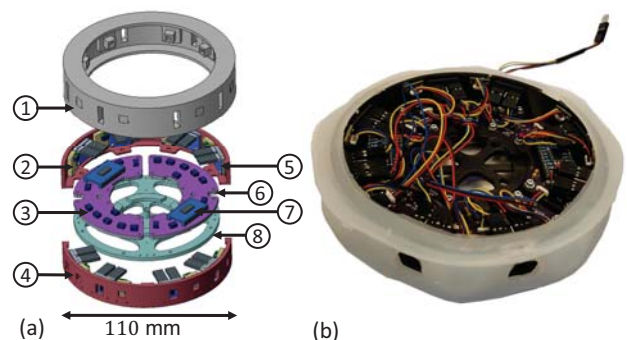

Fig. 2: (a) Exploded view of the sensing disk unit (SDU): 8 magnetic sensors ② and 8 time-of-flight sensors ⑤ are assembled in a radial pattern onto two half disks ④. The communication between the sensors and a master device (not shown) is achieved through an I^2C bus, via two multiplexers ⑦ mounted on a custom PCB ⑥. QWIIC I^2C connectors ③ are used for connection between the sensors and the PCBs, between the two internal PCBs of the SDU, and between consecutive SDUs. The PCBs and the two half rings are mounted onto core disk ⑧. A silicone sleeve ① encloses the magnets for Hall effect sensing and protects the disk. (b) Prototype of the SDU.

For force sensing and localized contact detection, the sensing unit is equipped with an array of eight programmable triaxis magnetic field sensors (Melexis, MLX90393) distributed around its circumference. To achieve the Hall effect, eight cylindrical magnets (KJ magnetics, Grade N52, 1/16 in.

diameter, 1/32 in. thickness) are embedded in the silicone sleeve in a circumferential pattern that matches that of the magnetic field sensors. The magnets are positioned 5.5 mm away from the MLX90393 sensor, including a 2 mm air gap. An external force at the circumference of the SDU displaces the magnet, and thus changes the magnetic field reading on the MLX90393 sensor. The change in magnetic field is proportional to the applied force. The working principle of these types of sensors is detailed in [22]. The calibration between the force sensor readings and the intensity of the magnetic field is presented in Section III-B.

In addition to housing the magnets for Hall effect sensing, the silicone sleeve protects the disk unit from harsh interactions with both the environment and the human user. This sleeve was fabricated by casting liquid silicone rubber (Dragon Skin FX pro, Advanced Reynolds) into a two-part custom mold. With a shore 2A hardness, this elastomer is both flexible enough to detect the motion of the embedded magnet, and robust enough to withstand rolling contact with the environment. To ensure a tight fit around the sensing disk, the inner diameter of the silicone sleeve was set to be 75% of the outer diameter of the disk. The upper and lower lips of the sleeve prevent axial motion relative to the disk. Furthermore, the inner surface of the sleeve is designed with square extrusions that fit into matching holes on the disk. These extrusions have the dual function of a) preventing tangential motion relative to the disk, and b) aligning the magnets with the Hall effect sensors. The silicone sleeve also features windows for the operation of the ToF sensors.

For communication between the different sensors and a microcontroller (Teensy 3.5), we used inter-integrated circuit (I^2C) communication protocol. This protocol enables communication with up to 128 peripheral devices in a bus configuration, as long as each device has a unique 7-bit address. The VL6180X sensor has the I^2C address 0×29, and the MLX90393 sensor can be hardcoded to up to 16 individual I^2C addresses. The integration of these sensors onto a continuum segment with 10 spacer disks requires communication with 80 of each type of sensors. To communicate with each sensor while bypassing the challenge of non-unique I^2C addressing, we use a TCA9548A 1-to-8 I^2C multiplexer (Texas Instruments). Given that this multiplexer can be hardwired to up to eight different addresses (0×70 to 0×77), and that the Teensy 3.5 master enables the use of three separate I^2C buses, up to 192 (8 sensors per multiplexers $\times$ 8 multiplexers $\times$ 3 I^2C buses) same-address devices can individually addressed. Our strategy for communicating with 10 SDUs on a continuum segments is illustrated in Fig. 3.

For the physical setup of the I^2C bus, we used QWIIC I^2C connectors (Sparkfun Electronics) to plug the sensors onto the custom multiplexer PCBs, to connect the two PCBs on each disk to each other, and to connect each SDU to its neighbors on the continuum segment. As a result, only one cable, with four signals (data signal (SDA), a clock signal (SCL), power (Vin), and ground (G)) is required for communication between the SDUs and the master device.
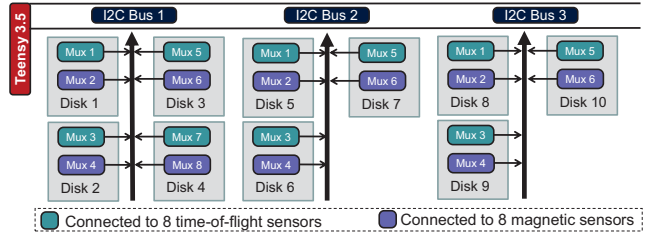

Fig. 3: Strategy for I^2C communication with 80 same-address time-of-flight sensors and 80 same-address magnetic sensors, distributed on 10 disks of a continuum robot.

III. Sensor Array Characterization

A. Proximity Sensing Characterization

To characterize the proximity sensors, a custom Cartesian stage robot was used with a rotary stage (Sherline™) that concentrically supported the SDU, as depicted in Fig. 4. The goal of the experiments was to determine the detection cone angles, the distance sensing error, sensitivity of the sensors to changes in object colors and reflectivity, and the repeatability of measurements across different sensors on the SDU.
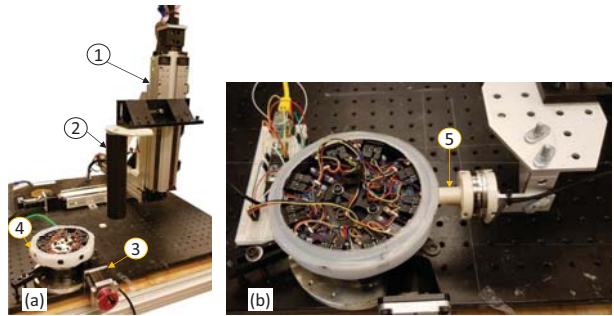

Fig. 4: (a) Time-of-flight sensor characterization experimental setup: ① custom Cartesian robot, ② 50.8 mm diameter Delrin rod, ③ rotary stage, ④ SDU. (b) Hall effect sensor characterization experimental setup: ⑤ ATI Nano 43 force sensor.

Referring to Fig. 4, a 2 in (50.8 mm) diameter Delrin rod was attached to the robot's end-effector during the sensor characterization experiments. This diameter was chosen to approximate the size of a human wrist, the narrowest portion of the human anatomy likely to come into the path of a robot during a collaborative task. While a finger is narrower than the wrist, it is unlikely that a single finger is detected without detecting the rest of the palm.

The custom Cartesian robot was comprised from ballscrew-driven Parker™ 404XR series linear stages with 200 mm stroke. Each stage was actuated using a 90 Watt brushed DC motor (Maxon™ RE35 #273754) equipped with a 500 counts per revolution encoder (Maxon™ HEDL #110512). A computed torque controller was tuned and verified to provide motion accuracy of better than 30 μm in each direction.

As a first step, the location and orientation of the SDU was registered to the robot frame by driving a peg centered

at the bottom of the Delrin rod into a matching hole on the SDU. This process was repeated for two angles ($\theta_{rs} = 0°$ and $\theta_{rs} = 90°$) of the rotary stage, thereby allowing the registration of the center of the disk. The angle of the SDU was read from the rotary stage, which afforded a precision of better than 0.1 degrees. Following registration, the robot swept the rod in front of a selected proximity sensor to compare the proximity readings to the rod's actual distance from the sensor. The rotary stage was positioned at the corner of the Cartesian robot's workspace in order to maximize its usable workspace. The rotary stage was used to rotate the SDU such that its detection cone was entirely within the workspace of the robot.

Next, a trajectory was planned to sweep the Delrin rod through the detection cone of the sensor (Fig. 5). Starting at a position touching the SDU, but out of the detection cone of the sensor of interest, the rod was swept at constant radius for $\pm15°$ about the center of the SDU. The rod was stopped every 5 mm arc length to await 20 readings from the ToF sensor. After the full 30°, the sweeping radius was increased by 1 mm and then again swept 30° at constant radius. This process was completed until the center of the rod was 135 mm radially from the SDU outer diameter.
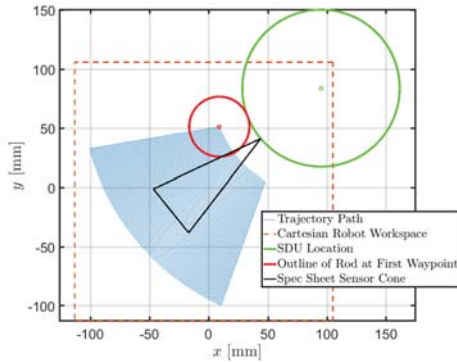

Fig. 5: Trajectory of the cartesian stage robot during the ToF sensor characterization experiment.

To determine the sensitivity of the readings to changes in color and reflectivity, the experiment was repeated with three types of Delrin rods: a bare glossy black rod, a rod covered with matte black tape, and a rod covered with a matte light-blue tape. These three tests were performed on two different sensors to validate repeatability of the results across sensors. For each trajectory waypoint, the mean sensor ranging error, e was calculated using (1).

$$e = (\|\boldsymbol{p}_{sensor} - \boldsymbol{p}_{rod}\| - r_{rod}) - \bar{d} \qquad (1)$$

where $\boldsymbol{p}_{sensor}$ and $\boldsymbol{p}_{rod}$ are the positions of the sensor and rod in robot frame, r_{rod} is the radius of the rod, and $\bar{d}$ is the mean ranging measurement at the given pose.

Figure 6 reports the results of these experiments. Figure 6(a) shows the colorbar plots for the relative error in the ranging value on top. These figures show qualitatively the effects of surface reflectivity on the error. It can be seen the glossy reflecting surface decreased the width of the detection cone. Figure 6(b) plots the ranging errors on a polar plot. On this figure, it can be seen that the detection cone angle is $\pm11.9°$ for the glossy black surface and $\pm16.5°$ for the matte black reflecting surface. Figure 6(c) shows the plots of the ranging error in 3D view (top) and in a side view (bottom). These figures show that within the detection cone for the matte black rod, the errors were bounded between 0.01 mm and 12.5 mm. For the glossy black rod, the errors were bounded between 0.019 mm and 15.6 mm. It is also noticeable that these sensors exhibited less error when matte surface was used, as illustrated in Fig. 6(c) and (d). While the figure shows the results for one sensor and for one color, the results showed similar trends between different sensors. When repeating the experiment with the Delrin rod covered with matte blue tape, we obtained similar results to the matte black surface. These results are omitted for space considerations.

B. Contact and Force Sensing Characterization

The MLX90393 Hall effect sensors measure magnetic flux density of the embedded magnets. When an external force is applied to the SDU, the position of the magnet changes relative to the stationary Hall effect sensor. This relative motion causes a change in the magnetic field intensity measured by the sensor. We conducted an experiment to evaluate the relationship between the magnetic field intensity and the magnitude of the applied force, along with the repeatability and hysteresis of the sensors. The experimental setup is shown in Fig. 4 (b). An ATI Nano 43 force sensor was attached to the custom Cartesian robot described in the previous section.

Starting at the surface of the SDU, the Cartesian robot was programmed to move the force sensor radially inward against the disk, in increments of 0.1 mm, until a radial force of 10 N was reached. At this point, the robot was commanded to return to its starting position, using the same incremental motion, in the reverse direction. This trajectory was repeated 10 times for each Hall effect sensor. The force sensor data F, the field intensity values B, and radial position x of the force sensor were recorded in Simulink Real Time™.

The results from the force calibration experiment are presented in Fig. 7(a). The Hall effect sensors exhibit a fairly repeatable quadratic relationship between magnetic field intensity B and applied force F in the normal direction. However, it is noticeable that each sensor has a unique field intensity bias. Therefore, moving forward, an un-biasing routine will need to be implemented on startup. The tangential components of the applied force will also be evaluated and calibrated in future works. Fig. 7(b) shows the hysteresis curves for Hall effect sensor S4. Calibration curves were evaluated from data points acquired in both directions of the force sensor motion. The RMS error between the *forward* and *reverse* calibration curves was 0.55 N/mT.
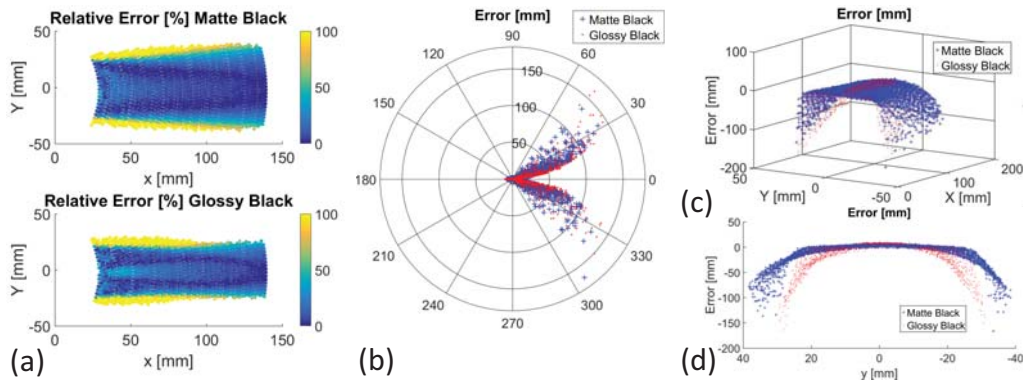
Fig. 6: Sensor error characterization: (a) relative error colormap, (b) polar plot of absolute error as a function of angle of line of sight to the detected object, (c) 3D plot of sensor error, (d) side view of the 3D plot of sensor error.
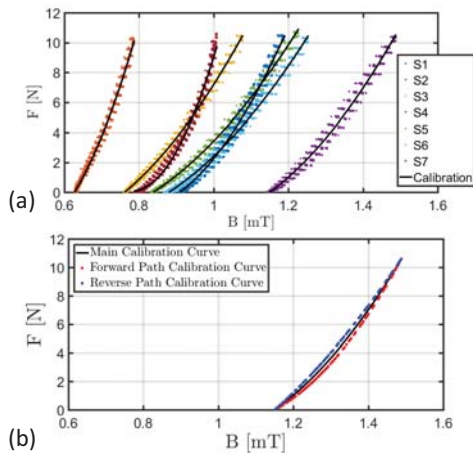

Fig. 7: (a) Magnetic sensor force calibration results for sensors around the SDU. (b) Hysteresis curves of the S4 MLX90393 sensor.

IV. EXPERIMENTS WITH MAPPING AND BRACING

The performance of the SDU was evaluated on a PUMA 560 industrial robot using a custom real-time controller running on Simulink Real-time. This robot was used for the tasks of mapping an environment and bracing against a surface. The SDU was mounted on the output flange of the manipulator, while the microcontroller/ethernet board reading the sensor ring data was mounted on the robot's "forearm" link. The SDU data, which includes the ToF ranges and the magnetic sensor readings, was sent via user datagram protocol (UDP) to a MATLAB script that generated desired end-effector poses or twists depending on the task. A computer running MATLAB Simulink Real-Time received the desired end-effector poses/twists and commanded motor voltages in real-time at 1 kHz using computed torque control.

A. Finding Admissible Bracing Surfaces

In an unstructured environment, the ToF sensors on the sensor ring can be used to identify suitable surfaces for bracing. To this end, we show an experiment where the ToF sensor were used to identify planes of interest. The PUMA

was controlled in task space using a resolved-rates algorithm to move slowly along a straight line while twisting the end-effector $\pm$ 90°and recording range data from all ToF sensors. In the future, continuum robots equipped with SDUs will be able to achieve this rotation using coordinated control of their backbones to achieve rotation about their backbone as was demonstrated in miniature continuum robots [23], [24].

The scanned geometry was a wooden planar surface with a small wooden block placed as shown in Fig. 8 (a) and (c). The resulting point cloud is shown in Fig. 8 (b). We applied a random sample consensus (RANSAC) based plane-extraction method as implemented in MATLAB's pcfitplane function, which is an iterative method to estimate the parameters of a potential geometry model in the generated point-cloud data. With prior knowledge that the geometry being scanned was horizontally placed, we fit the surface onto a plane with a plane-normal vector of $v = [0, 0, 1]$. We then ignore the points already assigned to a plane and continue to fit other planes with the remaining points.

Figure 8(c) shows green data points that were assigned to one plane and red data points that were assigned to a second plane. As part of our experiment, our goal was to identify a surface with a continuous planar area of at least 150 mm $\times$ 150 mm. This criterion was defined as a safety measure to protect the SDU's from resting on small corners/thin beams that may be present in a semi-structured environment. Using this criterion, the green surface was identified as a suitable surface for bracing while the red surface was inadmissible.

B. Utilizing Multi-modal Sensing for Bracing

The PUMA 560 (with the SDU attached) was also used to demonstrate the utility of the proposed SDU for robotic bracing against an environment. In addition to using the Hall effect touch sensors to stop the robot's motion when contact was detected, the proximity sensors were used to reduce the robot's velocity as the bracing surface was being approached. This multi-modal sensing capability can reduce risk to the environment and humans when there is significant uncertainty in the environment.

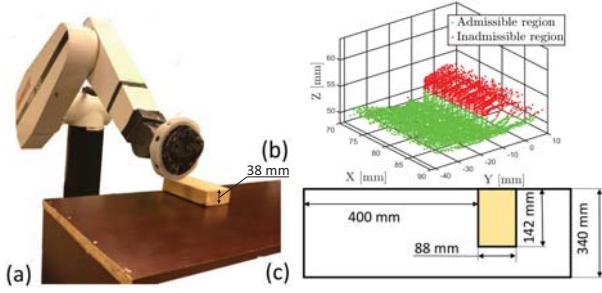The bracing surface was the same flat surface used in

Fig. 8: Scanning experiment: (a) the PUMA robot scanning with the sensor disk, (b) point cloud results after scanning, and (c) dimensions of geometry being scanned.

the mapping experiments above, but without the additional wooden block. The end effector was first initialized to a pose above the surface with the disk aligned to be normal to the surface (Fig. 9 (a)). The robot was then commanded to move downward while using the ToF sensors to regulate its velocity according to:

$$\|\boldsymbol{v}\| = \begin{cases} \frac{d_e}{d_{max}}(v_{max} - v_{min}) + v_{min} & d_e < d_{max} \\ v_{max} & d_e \geq d_{max} \end{cases} \quad (2)$$

$$d_e = d\cos(\theta) \quad (3)$$

where $\|\boldsymbol{v}\|$ is the norm of the velocity vector, d_e is the estimated distance to the surface, d is the measured distance from the ToF sensor nearest to the surface, θ is the angle of the ToF sensor relative to the surface normal, and d_{max} is the absolute maximum distance the sensor can detect. By reducing the velocity as d_e approaches zero, the touch sensors are able to more precisely detect the instance of contact. In the experiment, we set $v_{max} = 50$ mm/s and $v_{min} = 0.25$ mm/s. Once contact was detected on a magnetic sensor, the motion was stopped (Fig. 9(b)). At this instant, the constrained instantaneous kinematics becomes:

$$\dot{\boldsymbol{q}} = \mathbf{J} \begin{bmatrix} [\mathbf{r}_c]^{\times} \hat{\boldsymbol{z}} \\ \hat{\boldsymbol{z}} \end{bmatrix} \omega_z \quad (4)$$

where $\dot{\boldsymbol{q}}$ is the vector of joint speeds, $\mathbf{J}$ is the robot's geometric Jacobian, $[\mathbf{r}_c]^{\times}$ is the skew-symmetric form of the vector from the center of the sensor ring to the point of contact, $\hat{\boldsymbol{z}}$ is the unit vector normal to the SDU, and ω_z is a scalar angular velocity about $\hat{\boldsymbol{z}}$. The kinematics in (4) reduces the manipulator's task space to a one degree-of-freedom no-slip roll motion. After making contact, we commanded the robot to move back and forth along the surface according to the kinematics in (4). Video snapshots from the multimedia extension showing this experiment are shown in Fig. 9.

C. Detecting Human Contact

Using the same programmed motion as in the above bracing experiment, we also demonstrated the use of the sensor ring to detect human contact. Figure 10 shows video snapshots of this experiment taken from the multimedia extension, showing the robot moving with constant velocity and detecting human contact using one of its Hall effect sensors. The ability to detect contact is limited for a single
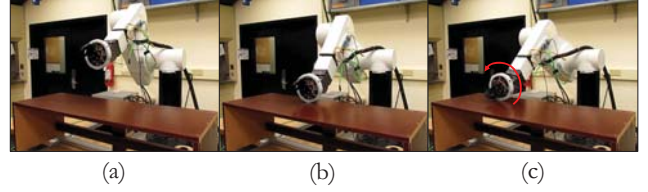

Fig. 9: Video snapshots showing (a) approaching the bracing surface, (b) detecting contact using magnetic sensors, and (c) no-slip rolling along the surface.
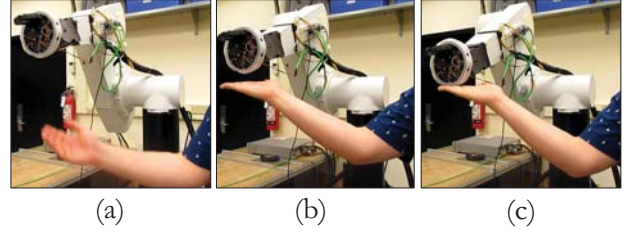

Fig. 10: Video snapshots showing (a) robot moving with constant velocity, (b) slowing down near human contact, and (c) stopping motion after detecting contact.

disk, however in our planned embodiment in a continuum segment as shown in Fig. 1, whole-body localization of contact will be possible.

V. DISCUSSION

In our current implementation, every sensor on the SDU is read one at a time on a single I^{2}C bus using a multiplexer. As a result, the maximum combined communication and sampling rate for the whole SDU was limited to approximately 4 Hz. Due to this slow sampling rate, the PUMA robot could only be used at slow end-effector velocities during the mapping and contact detection experiments. If the robot was moving quickly, the control system could not react fast enough to prevent high speed collision with the environment. In future work, we will investigate methods to allow for increased sampling frequencies such as alternative wiring architectures and/or communication protocols.

VI. CONCLUSION

In this paper, we proposed the replacement of passive spacer disks of continuum robots with multi-modal sensing disk units for safe human-robot interaction and mapping. We presented the design of the sensing unit, characterized the accuracy of the detection cones, and presented preliminary characterization of the Hall effect force sensing. Experiments on an industrial manipulator demonstrated the use of the SDU for mapping the environment, identifying potential bracing surfaces, and utilizing the multi-modal sensing capabilities to establish a bracing contact against an environment.

We believe that the multi-modal sensory perception provided by this SDU design will allow *in-situ* collaborative robots to be safely deployed in confined spaces and intelligently interact with the environment and human users. Future work includes integration and evaluation of multiple SDUs in the structure of a continuum manipulator.

REFERENCES

[1] Occupational Safety and Health Administration. (2017) Prevention of work-related musculoskeletal disorders, [online]. https://www.osha.gov/pls/oshaweb/owadisp.show_document?p_table=UNIFIED_AGENDA&p_id=4481.

[2] M. Zinn, O. Khatib, B. Roth, and J. K. Salisbury, "Playing it safe [human-friendly robots]," *IEEE Robotics & Automation Magazine*, vol. 11, no. 2, pp. 12–21, 2004.

[3] A. De Luca, A. Albu-Schaffer, S. Haddadin, and G. Hirzinger, "Collision detection and safe reaction with the dlr-iii lightweight manipulator arm," in *2006 IEEE/RSJ International Conference on Intelligent Robots and Systems*. IEEE, 2006, pp. 1623–1630.

[4] R. Bloss, "Collaborative robots are rapidly providing major improvements in productivity, safety, programing ease, portability and cost while addressing many new applications," *Industrial Robot: An International Journal*, vol. 43, no. 5, pp. 463–468, 2016.

[5] G. Robinson and J. B. C. Davies, "Continuum robots-a state of the art," in *Proceedings 1999 IEEE international conference on robotics and automation (Cat. No. 99CH36288C)*, vol. 4. IEEE, 1999, pp. 2849–2854.

[6] K. Xu, N. Simaan *et al.*, "An investigation of the intrinsic force sensing capabilities of continuum robots," *IEEE Transactions on Robotics*, vol. 24, no. 3, pp. 576–587, 2008.

[7] D. C. Rucker and R. J. Webster, "Deflection-based force sensing for continuum robots: A probabilistic approach," in *Intelligent Robots and Systems (IROS), 2011 IEEE/RSJ International Conference on*. IEEE, 2011, pp. 3764–3769.

[8] W. Wei and N. Simaan, "Modeling, Force Sensing, and Control of Flexible Cannulas for Microstent Delivery," *Journal of Dynamic Systems, Measurement, and Control*, vol. 134, no. 4, p. 041004, 2012.

[9] S. Hasanzadeh and F. Janabi-Sharifi, "Model-Based Force Estimation for Intracardiac Catheters," *IEEE/ASME Transactions on Mechatronics*, vol. 21, no. 1, pp. 154–162, 2016.

[10] R. Xu, A. Yurkewich, and R. V. Patel, "Curvature, torsion, and force sensing in continuum robots using helically wrapped fbg sensors," *IEEE Robotics and Automation Letters*, vol. 1, no. 2, pp. 1052–1059, 2016.

[11] A. Bajo and N. Simaan, "Kinematics-based detection and localization of contacts along multisegment continuum robots," *IEEE Transactions on Robotics*, vol. 28, no. 2, pp. 291–302, 2012.

[12] J. Rajruangrabin and D. O. Popa, "Enhancement of manipulator interactivity through compliant skin and extended kalman filtering," in *Automation Science and Engineering, 2007. CASE 2007. IEEE International Conference on*. IEEE, 2007, pp. 1111–1116.

[13] D. Silvera-Tawil, D. Rye, and M. Velonaki, "Artificial skin and tactile sensing for socially interactive robots: A review," *Robotics and Autonomous Systems*, vol. 63, pp. 230–243, 2015.

[14] Z. Kappassov, J.-A. Corrales, and V. Perdereau, "Tactile sensing in dexterous robot hands," *Robotics and Autonomous Systems*, vol. 74, pp. 195–220, 2015.

[15] M. Kaboli, D. Feng, K. Yao, P. Lanillos, and G. Cheng, "A tactile-based framework for active object learning and discrimination using multimodal robotic skin," *IEEE Robotics and Automation Letters*, vol. 2, no. 4, pp. 2143–2150, 2017.

[16] R. Patel, R. Cox, and N. Correll, "Integrated proximity, contact and force sensing using elastomer-embedded commodity proximity sensors," *Autonomous Robots*, vol. 42, no. 7, pp. 1443–1458, 2018.

[17] P. Mittendorfer and G. Cheng, "Humanoid multimodal tactile-sensing modules," *IEEE Transactions on robotics*, vol. 27, no. 3, pp. 401–410, 2011.

[18] M. Sohgawa, A. Nozawa, H. Yokoyama, T. Kanashima, M. Okuyama, T. Abe, H. Noma, and T. Azuma, "Multimodal measurement of proximity and touch force by light-and strain-sensitive multifunctional mems sensor," in *SENSORS, 2014 IEEE*. IEEE, 2014, pp. 1749–1752.

[19] S. Hirai, K. Naraki *et al.*, "Fabric interface with proximity and tactile sensation for human-robot interaction," in *Intelligent Robots and Systems (IROS), 2016 IEEE/RSJ International Conference on*. IEEE, 2016, pp. 238–245.

[20] I. A. Gravagne and I. D. Walker, "Kinematic transformations for remotely-actuated planar continuum robots," in *Robotics and Automation, 2000. Proceedings. ICRA'00. IEEE International Conference on*, vol. 1. IEEE, 2000, pp. 19–26.

[21] N. Simaan, R. Taylor, and P. Flint, "A dexterous system for laryngeal surgery," in *Robotics and Automation, 2004. Proceedings. ICRA'04. 2004 IEEE International Conference on*, vol. 1. IEEE, 2004, pp. 351–357.

[22] T. Paulino, P. Ribeiro, M. Neto, S. Cardoso, A. Schmitz, J. Santos-Victor, A. Bernardino, and L. Jamone, "Low-cost 3-axis soft tactile sensors for the human-friendly robot vizzy," in *Robotics and Automation (ICRA), 2017 IEEE International Conference on*. IEEE, 2017, pp. 966–971.

[23] N. Simaan, K. Xu, W. Wei, A. Kapoor, P. Kazanzides, R. Taylor, and P. Flint, "Design and integration of a telerobotic system for minimally invasive surgery of the throat," *The International journal of robotics research*, vol. 28, no. 9, pp. 1134–1153, 2009.

[24] J. Ding, R. E. Goldman, K. Xu, P. K. Allen, D. L. Fowler, and N. Simaan, "Design and coordination kinematics of an insertable robotic effectors platform for single-port access surgery," *IEEE/ASME transactions on mechatronics*, vol. 18, no. 5, pp. 1612–1624, 2013.